(p, γ) Resonance-Curve Shapes and Measurements of Resonance Energies with H_1^+ Beams

R. O. BONDELID AND J. W. BUTLER*

Nucleonics Division, U. S. Naval Research Laboratory, Washington, D. C.

(Received 3 October 1962; revised manuscript received 11 February 1963)

During the preparation of a new precise absolute energy scale for nuclear reaction accelerators, some "anomalies" were observed in the behavior of (p,γ) resonances. These observations led to an exhaustive investigation of (p,γ) yield-curve shapes and detailed interpretation of these shapes in terms of physically significant quantities such as resonance energy and resonance width. Most of the measurements have been made with respect to the 992-keV resonance in the $Al^{27}(p,\gamma)$ reaction, but other reactions have also been used. A list of the anomalies observed includes (1) the failure of the peaks of thin-target resonance yield curves to be shifted from resonance energy by as much as half the target thickness, (2) the displacement of the midpoint of the rise of thick-target yield curves to bombarding energies below the resonance energy, (3) the "overshoot" of the yield curve for thick targets forming a hump above the thick-target plateau, (4) the obtaining of apparently different intrinsic resonance widths for the same resonance and from the same thick target at different times separated by a few weeks, and (5) the obtaining of significantly different thick-target yield-curve shapes from the same target in two different orientations with respect to the beam. The anomalies are all satisfactorily explained on the basis of fluctuations in energy loss of the bombarding protons as they penetrate the target. The theory used was chiefly developed by Symon. Detailed numerical integrations of the formal yield equation have been made, and in most cases very good fits have been made with the experimental data. The information gained from this investigation is applied to energy calibrations resulting in precise best values for the following narrow (p,γ) resonances: $Al^{27}(p,\gamma)Si^{28}$ reaction, 991.91 ± 0.30 and 1317.19 ± 0.40 keV; $C^{13}(p,\gamma)N^{14}$ reaction, 1747.06 ± 0.53 keV; $Ni^{58}(p,\gamma)Cu^{59}$ reaction, 1423.64 ± 0.43 and 1843.45 ± 0.56 keV. The displacement of the midpoint of the rise of a thick-target yield curve from the resonance energy E_r as a function of the resonance width Γ is discussed, and a typical curve of this relationship is shown. The overshoot or hump height for a thick target as a function of Γ is also discussed, and a curve is shown.

I. INTRODUCTION

A POINT on the energy calibration scale for nuclear reaction accelerators is defined by an unambiguous characteristic of a yield curve as a function of bombarding energy. The use of (p,γ) resonance reactions for calibration purposes is quite common because of the experimental simplicity of the measurements and also because of the relative lack of ambiguity in the interpretation of the data if the resonance is sharp ($\Gamma \sim 100$ eV or less). Excellent comprehensive summaries of the procedures used in the interpretation of (p,γ) resonance data have been written by Fowler *et al.*[1] (1948) and Gove[2] (1959).

It has become commonly accepted practice to apply the following rules to the interpretation of (p,γ) resonance reaction data. (1) The position of the experimentally observed peak of a resonance is shifted from resonance energy by half the target thickness, in terms of energy loss. (2) The thick-target yield curve has essentially the shape of the integral of the Breit–Wigner dispersion relation and the incident beam-energy distribution, and is, therefore, symmetric about the midpoint of the rise. (3) The resonance energy is located at the midpoint of the rise in the thick-target yield curve. These concepts have been considered to be valid for resonances narrow enough for the stopping power of the target material and the Coulomb penetrability of

protons to be considered constant over the effective energy range of the resonance. These rules of interpretation had been extended to include the hydrogen molecular ion beam, the generally held opinion being that one could use this beam in much the same way that one uses the proton beam, the required energy for the hydrogen molecular ion being twice that necessary for the proton plus the energy carried by the electron.

Historically, the present series of investigations was initiated by the observation of an apparent nonlinearity in the NRL 2-m radius electrostatic beam-energy analyzer. The apparent energy of the 992-keV resonance in the $Al^{27}(p,\gamma)$ reaction, determined from the midpoint of the rise in the thick-target yield curve with the hydrogen molecular ion beam, was lower than anticipated from the measurements with the proton beam, the amount of the "discrepancy" being about 0.05%.[3] All of the usual corrections, the relativistic effect, internal and external magnetic fields, and energy carried by the electron, were made to the raw experimental data before the situation was labeled a discrepancy.

Because of the critical relationship of this observation to the program of preparation of a new precision absolute energy calibration scale,[4-8] considerable effort

---

* Present address: Department of Physics and Astronomy, Michigan State University, East Lansing, Michigan.

[1] W. A. Fowler, C. C. Lauritsen, and T. Lauritsen, Rev. Mod. Phys. **20**, 236 (1948).

[2] H. E. Gove, in *Nuclear Reactions*, edited by P. M. Endt and M. Demeur (North-Holland Publishing Company, Amsterdam; Interscience Publishers Inc., New York, 1959), Vol. 1, Chap. VI.

[3] R. O. Bondelid, J. W. Butler, and C. A. Kennedy, Bull. Am. Phys. Soc. **2**, 381 (1957).

[4] K. L. Dunning, J. W. Butler, and R. O. Bondelid, Phys. Rev. **110**, 1076 (1958).

[5] R. O. Bondelid and C. A. Kennedy, Phys. Rev. **115**, 1601 (1959); also NRL Report 5083, 1958 (unpublished).

[6] R. O. Bondelid, J. W. Butler, C. A. Kennedy, and A. del Callar, Phys. Rev. **120**, 887 (1960).

[7] R. O. Bondelid, J. W. Butler, and C. A. Kennedy, Phys. Rev. **120**, 889 (1960).

[8] J. W. Butler and R. O. Bondelid, Phys. Rev. **121**, 1770 (1960).

was expended in attempts to understand the nature of the observed discrepancy. The program was extended to include careful observations of (p, γ) resonance yield curves with both the hydrogen molecular ion (H_2^+) beam and the proton (H_1^+) beam. As sometimes happens when an intensive effort is made to discover the nature of one "discrepancy," or "anomaly," other "anomalies" are found. One of these deviations, a peak or "hump" at the top of the H_1^+ beam thick-target yield-curve leading edge, was reported by del Callar.[9]

For both the H_1^+ and H_2^+ beams deviations from the rules listed above were found. For both beams the most important deviations are (1) the failure of the peaks of thin-target yield curves to shift from resonance energy by half the target thickness in energy loss units and (2) marked asymmetries in the thick-target yield curves.

The energy discrepancy with the H_2^+ beams has been subsequently reported by workers at two other laboratories.[10,11] The Oslo group reported the observation of the H_2^+ energy discrepancy and asymmetries in the H_2^+ beam thick-target yield curve. The Wisconsin group initiated a similar program and have published their work.[12–21]

The present paper is a report of the detailed shapes of (p, γ) yield curves induced by the H_1^+ beam and the detailed interpretation of these shapes in terms of physically significant quantities such as resonance energy and resonance width.

II. EXPERIMENTAL APPARATUS

The positive-ion-beam acceleration was performed by the NRL 5-MV Van de Graaff Accelerator; the beam analysis was accomplished by a high-resolution 2-m-radius electrostatic beam-energy analyzer; and the proton-capture gamma rays were detected by a 3-in. diam$\times$3-in. NaI(Tl) scintillation crystal with associated electronic equipment.

The bombarding beam, after emerging from the accelerator, passed through a magnetic beam-momentum analyzer (40° deflection) for preliminary energy selection and mass-component separation. Then the ion beam passed through the precision electrostatic analyzer (90° deflection), whose input slit-defining jaws were common with the output slit-defining jaws of the magnetic analyzer. The fine-energy stabilization of the accelerator was achieved by the use of electrical signals from these jaws controlling the amount of corona current to the high-voltage terminal through the insulating gas of the accelerator. The entire system is described in detail in other communications.[5,22]

The NaI(Tl) crystal was placed at various orientations with respect to the target and bombarding beam during the various phases of the series of experiments, a typical position was at 90° with respect to the bombarding beam and in the horizontal plane containing the beam. A type-6363 multiplier phototube was optically coupled to the crystal, and its pulses were amplified and analyzed by a conventional linear amplifier and single-channel pulse-height analyzer. The analyzer window width was varied from time to time, but typical lower and upper settings were about 7 and 13 MeV.

The target holder formed a natural Faraday-type cup for beam-current collection, and the current was integrated by a conventional Higinbotham and Rankowitz circuit.[23]

III. TARGETS

During the early phases of the program of experiments, the aluminum targets were generally evaporated onto metallic backings such as silver or tantalum. The asymmetries in the thin-target yield curves from these metallic-backed targets indicated nonuniformities in target thickness, and these asymmetries made it difficult to observe and interpret other effects. To diminish effects due to target nonuniformities, a target improvement program was undertaken with the following procedure being evolved.

The basic backing material was chosen to be microscope slide glass (1 mm thick) cut into disks of diameter 15/32 in. The disks were thoroughly cleaned, and a layer of copper approximately thick enough to stop a 1-MeV proton was deposited by evaporation in vacuo.

The purpose of the copper plating over the glass was threefold: (1) to conduct heat away from the bombarded area of the aluminum target and thus prevent target damage due to high temperatures during positive-ion-beam bombardment, (2) to conduct away electric charge and thus prevent the buildup of electric potential on the target, and (3) to reduce the (p, γ) yield from the backing material.

The aluminum target material was usually deposited

[9] A. del Callar, Master of Science Thesis, Catholic University of America, 1959 (unpublished).

[10] S. L. Andersen, K. Gjötterud, T. Holtebekk, and O. Lönsjö, Nucl. Phys. 7, 384 (1958).

[11] P. F. Dahl, D. G. Costello, and W. L. Walters, Nucl. Phys. 21, 106 (1960).

[12] P. F. Dahl, D. G. Costello, and W. L. Walters, Bull. Am. Phys. Soc. 5, 406 (1960).

[13] D. G. Costello, W. L. Walters, and R. G. Herb, Bull. Am. Phys. Soc. 6, 250 (1961).

[14] W. L. Walters, D. G. Costello, J. G. Skofronick, D. W. Palmer, W. E. Kane, and R. G. Herb, Phys. Rev. Letters 7, 284 (1962).

[15] H. W. Lewis, Phys. Rev. 125, 937 (1962).

[16] D. G. Costello, W. L. Walters, J. G. Skofronick, D. W. Palmer, W. E. Kane, and R. G. Herb, Bull. Am. Phys. Soc. 6, 430 (1961).

[17] W. L. Walters, D. G. Costello, J. G. Skofronick, D. W. Palmer, W. E. Kane, and R. G. Herb, Bull. Am. Phys. Soc. 6, 431 (1961).

[18] W. L. Walters, D. G. Costello, J. G. Skofronick, D. W. Palmer, W. E. Kane, and R. G. Herb, Phys. Rev. 125, 2012 (1962).

[19] D. W. Palmer, J. G. Skofronick, D. G. Costello, W. E. Kane, and R. G. Herb, Bull. Am. Phys. Soc. 7, 301 (1962).

[20] J. G. Skofronick, D. W. Palmer, D. G. Costello, A. L. Morsell, W. E. Kane, and R. G. Herb, Bull. Am. Phys. Soc. 7, 301 (1962).

[21] D. G. Costello, W. E. Kane, A. L. Morsell, D. W. Palmer, J. G. Skofronick, and R. G. Herb, Bull. Am. Phys. Soc. 7, 301 (1962).

[22] K. L. Dunning, R. O. Bondelid, L. W. Fagg, C. A. Kennedy, and E. A. Wolicki, Report of NRL Progress, 1955, p. 8.

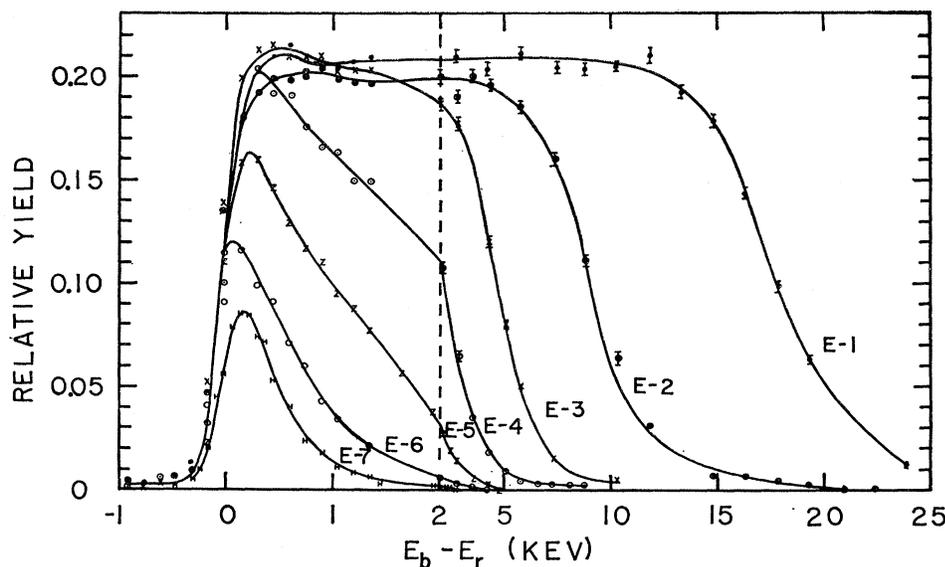[23] W. A. Higinbotham and S. Rankowitz, Rev. Sci. Instr. 22, 688 (1951).

FIG. 1. The experimental yield curves of the E-series aluminum targets near the resonance energy of 992 keV. The targets vary in thickness from 0.31 keV for E-7 to 17.8 keV for E-1, each different from its neighbor by about a factor of 2. Observe the failure of the peaks to shift as much as half the target thickness, and also the tendency for the yield to "overshoot" for the thick targets. Note the change in abscissa scale at 2 keV.

onto seven target blanks (with copper coatings) simultaneously. The distance of each disk from the aluminum was a factor of $\sqrt{2}$ different from that of its adjacent neighbors. The most important series of aluminum targets has a thickness range from 17.8 to 0.31 keV for 1-MeV protons. These targets are labeled E-1 through E-7 in descending order of thickness.

The entire series of experiments included observations of resonances in the $Ni^{58}(p,\gamma)$ reaction and a resonance in the $C^{13}(p,\gamma)$ reaction as well as resonances in the $Al^{27}(p,\gamma)$ reaction. Targets of Ni^{58} were prepared by electrodeposition onto silver backings. Thick targets of C^{13} were prepared by the heating of a molybdenum strip in an atmosphere of CH_3I, enriched to 40% C^{13}.

The target holder is similar to one previously described,[4] including a tube kept at liquid-nitrogen temperature enclosing the target. This tube is of critical importance to the present series of experiments for the following reasons: (1) the possible displacement of the energy of a resonance by the presence of a film of inert or contaminating material on the target face, (2) the background which such a film of contaminating material might contribute to the total counting rate, especially for the thinnest targets, and (3) the straggling effect on the bombarding beam of such a film. This last effect is much more serious than we had previously supposed, especially in connection with thick-target width measurements of very narrow resonances.

IV. EXPERIMENTAL RESULTS

During the course of the experiments several different values were used for the input and output slit widths of the electrostatic analyzer, resulting in several different beam-energy spreads. For most of the targets discussed below, the analyzer resolution was set to give a total beam-energy inhomogeneity of 0.04%. For some tar-

gets, the beam-energy inhomogeneity was increased a factor of 2.5, and for others it was decreased a factor of 2.

The H_1^+ beam yield curves for the 992-keV resonance and the family of targets E-1 through E-7 are shown in Fig. 1, whose abscissa values are the difference between the bombarding energy E_b and the resonance energy E_r. Note that there are two different abscissa scales on Fig. 1.

Several characteristics of narrow (p,γ) resonance yield curves may be seen from the family of curves in Fig. 1. The most striking characteristic perhaps is the failure of the experimental peaks to shift with target thickness according to rule (1) (see Introduction). Close scrutiny will reveal that there is a slight shift from target to target, which shift is to slightly higher energies, on the average, for thicker targets, but not by as much as half the target thickness. Even for the thick targets, the "peak" shifts only slightly. Thus, this behavior violates rule (2): that the yield curve for a thick target is symmetric about the midpoint. The peaks, or humps, appearing on the thicker target curves, while not so obvious in the curves of Fig. 1, are nonetheless real effects, and are more pronounced in subsequent figures. Figure 2, reproduced from del Callar's thesis,[9] shows the hump as observed for the 1317-keV resonance. Initially, it was not clear that these anomalies were not due to some experimental peculiarity; hence, an entire experimental program was devoted to efforts to determine the source or nature of these anomalies under the assumptions that the previously accepted rules were correct and that some facet of the experimental procedure or equipment was introducing aberrations or discrepancies. The reality of the failure of the peaks of the thin-target yield curves to shift with target thickness was established by the target improvement program. However, the target improvement program accentuated the hump. There-
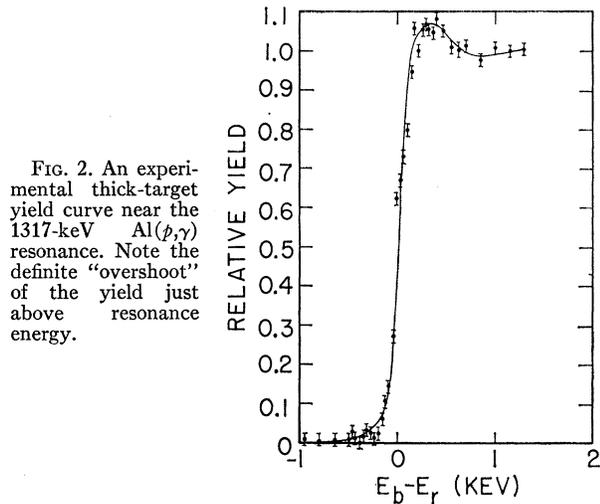
FIG. 2. An experimental thick-target yield curve near the 1317-keV Al(p,γ) resonance. Note the definite "overshoot" of the yield just above resonance energy.

more carefully we made the targets and the measurements, the more pronounced was the hump. We, therefore, concluded that the hump is a real effect in nature, and is in some way due to the nature of the mechanics of resonance reactions.

There were three ways that we could cause the hump to decrease significantly or disappear completely. (1) The use of a solid commercial sheet of aluminum as the target did not lead to the hump. (2) The use of old targets (more than about one month old) did not lead to the hump. (3) A target which showed the hump was rotated from its normal position (90° with respect to the bombarding beam) to 20°. This rotation had the effect of increasing the effective thickness (by a factor of 3) of all layers to the bombarding beam—any contaminant film on the surface, the oxidation layer, and the aluminum target itself. Thus, the effect of these surface films would be increased. At 20° the target showed essentially no hump, as shown in Fig. 3.

One further experimental condition which was varied was the beam-energy resolution by means of the analyzer-slit variations. The analyzer resolution (full width at half-maximum of the distribution) was varied from 0.01 to 0.05% with the result that the hump was clearly visible for all settings. There was a tendency for the hump to be more pronounced for the more homogeneous beams. This observation is consistent with another one—that the narrower resonances lead to more pronounced humps. Thus, the conditions which lead to the hump may be summarized: (1) pure, clean, and uniform targets, (2) narrow resonances, and (3) homogeneous bombarding beams.
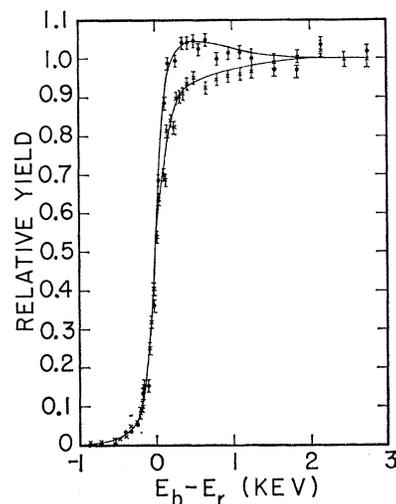
fore, further efforts were devoted to seeking the cause of the hump. A few of these efforts are listed as follows:

(1) A different source of aluminum was used for the target evaporations. (It was thought at the time that possibly a target contaminant in the source of aluminum was responsible for the hump.)

(2) Different backing materials were tried—tantalum, silver, copper sheet, and evaporated copper on glass—in an effort to determine whether a backing-material contaminant or the backing material was leading to the hump.

(3) Tantalum blanks and evaporated copper coatings on glass were bombarded in an effort to determine whether thin "targets" of aluminum existed on the walls of the target holder or elsewhere in the Van de Graaff vacuum system. If such targets did exist, they would give rise to a thin-target resonance curve superimposed on the thick-target step, thus leading to the hump on the thick-target yield.

(4) Possible target nonuniformities were considered. That is, if a portion (area) of the target were very thin compared to the rest of the target, it might give rise to a thin-target yield superimposed on the yield from the rest of the target.

(5) Another layer of aluminum was evaporated onto a thick target which showed the hump, and a new excitation curve was determined. The effort here was an attempt to determine whether the hump was due to some surface contaminant film or some other surface phenomenon such as oxidation. There were three possible results: two humps, one for each of the old and new surfaces; one hump displaced in energy, corresponding to the old surface; or one hump as if the entire target had been made in one operation. The result obtained was the last mentioned, thus eliminating any surface contaminant as the cause of the hump.

Neither these aforementioned efforts nor many others succeeded in eliminating the hump. On the contrary, the

FIG. 3. Experimental yield curves near $E_r=992$ keV for an aluminum target at two different orientations with respect to the bombarding proton beam. The data represented by the solid circles were obtained with the plane of the target perpendicular to the proton beam. The crosses represent the data obtained with the plane of the target making an angle of 20° with the proton beam. Note the lack of "overshoot" in the latter case, where the effective thickness of any contaminating film was increased by a factor of 3 over the former case.

One more anomaly which was observed does not directly violate any of the three previously listed rules governing the behavior of nuclear resonance phenomena, but it was unexpected and surprising nonetheless. The discovery of this anomaly arose from the efforts to make measurements of the widths of some very narrow resonances with thick targets. The resonances measured are the 992-keV resonance in the $Al^{27}(p,\gamma)$ reaction and the 1747-keV resonance in the $C^{13}(p,\gamma)$ reaction. It was observed that the "width" of any particular resonance was different for new and old targets. For example, the interquartile interval of the 992-keV resonance in the $Al^{27}(p,\gamma)$ reaction, as measured with a beam whose full width at half-maximum was 0.01%, was typically about 180 eV for a fresh target and about 210 eV for an old target.

The most reasonable explanation for such broadening would appear to be the formation of a film of inert material on the face of the target during a prolonged period of storage. However, such a film would be expected, on the basis of previous concepts, to displace the energy of the resonance. In the instances mentioned here, the energy of the resonance was not appreciably displaced by any such film, if one existed. However, an extremely thin layer of inert material might not displace the resonance energy for much the same reason that thicker "thin" targets do not cause a shift in the experimentally observed resonance peak. In a few instances, the same target was measured, first when new, and later when old. Again, the old target gave a wider experimental yield curve than the same one when new. In all cases, the old targets had been stored in clean containers.

V. INTERPRETATION OF ANOMALIES

The foregoing discussion has presented a number of experimental anomalies observed in connection with (p,γ) resonances. This section of the paper successfully explains these observations in terms of phenomena previously known but which were believed not to play a significant role in the interpretation of (p,γ) resonance measurements.

1. The Formal Yield Equation

The yield from a target may be represented by a multiple integral, with the integration over (1) the intrinsic shape of the resonance (Breit–Wigner dispersion relation), (2) the shape of the effective incoming beam-energy distribution, and (3) the target. Thus, the yield $y(E_b,t)$ at a bombarding energy E_b for a target of thickness t may be written

$$y(E_b,t)=n\int_{x=0}^{t}\int_{E_i=0}^{\infty}\int_{E=0}^{\infty}$$

$$\times\sigma(E)g(E_b,E_i)w(E,E_i,x)dEdE_idx, \quad (1)$$

where n is the number of target nuclei per unit volume,

$\sigma(E)$ is the nuclear-reaction cross section for a proton with energy E, $g(E_b,E_i)$ is the probability that a proton in the bombarding beam of average energy E_b will have an incident energy between E_i and E_i+dE_i, and $w(E,E_i,x)$ is the probability for a proton with incident energy between E_i and E_i+dE_i to have an energy between E and $E+dE$ when it is at a depth in the target between x and $x+dx$.

Let us now consider in detail the nature of each of the functions σ, g, and w. For narrow resonances, the Breit–Wigner dispersion relation $\sigma(E)$ is a simple analytic function of the difference between the resonance energy and the proton energy as it makes a nuclear pass.

In principle, the proton beam-energy distribution out of the electrostatic analyzer is triangular in shape if the ratio of the output slit width and the input slit width is set equal to the magnification of the analyzer and if the input distribution is uniform. However, there is some degree of smearing of this shape by the ripple in the voltage applied to the deflector plates. There is a further smearing of the effective beam-energy distribution by the thermal motion of the target nuclei in the target lattice structure ("Doppler" effect). For most of the data presented herein, the Doppler-effect contribution to the total effective beam width was comparable with that from the analyzer. Therefore, we have assumed that the effective incoming beam-energy distribution $g(E_b,E_i)$ can be represented to a sufficiently accurate approximation by a Gaussian shape with a standard deviation derived[5] from the triangular distribution, the ripple of the applied voltage, and the thermal motion of the target nuclei.

The resonance shape $\sigma(E)$ can be represented by an exact analytic form, and the incident effective beam-energy distribution $g(E_b,E_i)$ can be approximated satisfactorily. But the energy-loss distribution $w(E,E_i,x)$ is the result of a complicated statistical process which presents formidable mathematical difficulties.

2. Determination of the Function w

For some purposes it is reasonable to assume that the spread in energy of the beam remains constant as the beam traverses the target. This assumption implies that all particles in the beam lose energy at the same rate. The shape of the function $w(E,E_i,x)$ is then independent of the depth of penetration x, becoming simply $w=\delta[E-(E_i-kx)]$, where k is a constant equal to the stopping power (dE/dx) of the target material. Actually, it has been known for a long time that such is not the case because of statistical fluctuations in energy loss, but the simplified treatment has appeared justified for the treatment of (p,γ) resonance phenomena, thus leading to rules (1), (2), and (3) (see Introduction).

Landau[24] showed in 1944 that the distribution of energy losses of charged particles in penetrating moderately thin foils or targets was not Gaussian or sym-

[24] L. Landau, J. Phys. (U.S.S.R.) 8, 201 (1944).

metric, but instead was decidedly *asymmetric*, the value of the mean energy loss being significantly less than the average energy loss.

The difficulty with Landau's solution is that the asymmetry of his energy-loss distribution is independent of target thickness; and therefore, his solution can never agree with the Bohr–Bethe Gaussian solution which is known to be valid for thicker targets. The reason for the lack of validity of Landau's solution for thicker targets is due to certain assumptions he made in his mathematical analysis, and the range of validity of his results is predictable from these assumptions. Thus, there is an intermediate-thickness region in which neither the Gaussian distribution (thick foils) nor the Landau distribution (moderately thin foils) is applicable. Symon[25] bridged this gap in 1948 by solving the problem without making the restricting assumptions used by Landau. However, the results of Symon have not been widely appreciated. If they had, rules (1), (2), and (3) discussed in the Introduction would have been modified long ago for theoretical reasons before the modifications were necessitated by experiment.

Symon points out in his thesis that the distribution curves he has calculated are applicable to incident proton energies above 10 MeV and below 1000 MeV. Both Landau and Symon assumed that the velocity of the incoming particle is large compared to the velocity of the electrons with which the collisions occur. This condition is not completely satisfied for 992-keV protons impinging on aluminum because the K-shell electrons in aluminum have a velocity about 70% greater than that of 992-keV protons. However, the assumptions in the theory should hold reasonably well for the other electron shells. Another limitation of both solutions (Landau and Symon) is that neither applies to extremely thin targets because they both neglect fluctuations due to distant collisions (in which the atomic electrons cannot be treated as free). Even though the applicability of Symon's theory to the present case is somewhat questionable, the attitude taken in the present work is that this is the best theory available, and its usefulness is measured by how well it can satisfy the data.

Symon gives the most probable energy loss ΔT_p in terms of the silhouette area C of the electrons in one gram of target material, the density D of the target material, the average ionization potential $I(Z)$, the proton velocity βc, and the electron mass m_e.

$$\Delta T_p = \frac{2Cm_ec^2Dx}{\beta^2}\left[\ln\frac{4Cm_e^2c^4Dx}{(1-\beta^2)I^2(Z)} - \beta^2 + j\right]. \quad (2)$$

The dimensionless parameter j is a mathematical device which enables Eq. (2) to give the proper value for the most probable energy loss for any target thickness. In addition to the parameter j, Symon introduced two other dimensionless parameters b and λ. The param-

eter b is used primarily for convenience since its employment allows the multiple use of each set of tables. If we represent the coefficient of the bracketed term of Eq. (2) by the symbol ξ, then the quantity $b\xi$ has dimensions of energy and is related to the width of the distribution of energy losses. The parameter λ is related to the asymmetry of the distribution, and the range of its values are from 1.477 (corresponding to the Landau distribution) to zero (corresponding to Bethe's Gaussian distribution).

Another significant quantity related to the characteristics of the energy-loss distribution is the dimensionless ratio $G=\xi/E_m'$, where E_m' is the maximum energy transferable to a stationary free electron in a single collision. For the bombarding energies in which we are interested, $E_m'=2m_ec^2\beta^2/(1-\beta^2)$. Symon gives values of the parameters j, b, and λ as functions of G primarily and β secondarily. For any particular experimental situation, the values of G and β can be computed immediately. All factors, except x, involved in the energy-loss distribution for any particular (p,γ) resonance are fixed, and G is simply proportional to the depth x in the target. So we may think of the parameters j, b, and λ as functions of x.

Symon has calculated a family of curves $\varphi_\lambda(\Delta_w)$, which give the energy-loss distribution in terms of a dimensionless quantity Δ_w (which is the difference between the actual energy loss and the most probable energy loss, expressed in units of $b\xi$). In symbols $\Delta_w=(\Delta T-\Delta T_p)/b\xi$.

Since the parameters j, b, and λ are given as functions of the quantity G, the value of G serves as a useful criterion for the validity of the special-case solutions to the energy-loss problem. Landau's solution may be used if $G\ll1$, and Bethe's solution may be used if $G\gg1$. In the region of G values between about 0.1 and 10, neither of these two solutions is valid, and one must use Symon's solution, which is valid for all values of G.

Finally, the function $w(E,E_i,x)$, the probability that a proton whose incident energy is E_i will lose an energy of amount $\Delta T=E_i-E$ in going a distance x through the target, is $w(E,E_i,x)=\varphi_\lambda(\Delta_w)/b\xi$.

3. Integration of the Formal Yield Equation

The use of Symon's solution for the function w in the formal yield equation makes possible the calculation of the yield-curve shape for any target thickness and resonance width. However, the formal yield equation cannot be evaluated analytically because of the nature of the function w. Thus, the calculation of the yield-curve shape requires the use of a high-speed digital computer.

The many considerations involved in the evaluation of Eq. (1) are discussed elsewhere,[26] but one detail will be mentioned here because it involves a parameter

[25] K. R. Symon, Ph.D. thesis, Harvard University, 1948 (unpublished).

[26] R. O. Bondelid and J. W. Butler, NRL Report 5897 (unpublished).

qualitatively necessary for the comparison of the calculated yield curves with the data. Aluminum is very active chemically, and no vacuum is free of oxygen. Therefore, any aluminum target produced by presently available techniques is oxidized to some extent. But we do not know *a priori* the degree of these oxidations. Therefore, the degree of oxidation is regarded as an independent parameter whose value can be assigned in the computation of yield curves which may then be compared with the data.

4. Comparison of the Integrated Yield Equation with the Data from the E-Series Targets

In order to determine a starting point for the degree of volume oxidation to be assumed for the thick aluminum targets, we measured the thick-target resonance step for the 992-keV resonance using two different targets under the same detector geometry and other conditions. The first target was known to be essentially 100% Al_2O_3 (an anodized aluminum sheet), and the second target was target E-1 (thickest of the E series). The ratio of heights of the thick-target resonance steps for the Al_2O_3 target and target E-1 indicated that target E-1 was more than 90% aluminum. In order to simplify the starting point for the calculation, we assumed target E-1 to be 100% aluminum. As will be seen later it was necessary to modify this assumption; however, sufficient accuracy was obtained without introducing an iterative procedure. The quantity $I(Z)$ was taken to be 165 eV.[27] Under the assumptions that the integrated experimental yield is proportional to the number of aluminum atoms per unit area and that the targets consist of pure aluminum, the thicknesses in units of 10^{-5} cm of the remaining targets were found by comparisons of the values of the numerical integrations of their respective experimental yield curves with that of target E-1. The ratios of thicknesses for successively numbered targets thus determined were within a few percent of a factor of two.

In order to compare the experimental data with the calculated curves, we normalized the experimentally obtained yields by equating the areas under the experimental and calculated curves. This procedure normalized the ordinate values. The alignment of the abscissa values (i.e., the determination of resonance energy E_r) was accomplished visually.

The intrinsic resonance width Γ of the 992-keV resonance was taken to be 100 eV.[5]

There is a resonance[28] of relative intensity 4%, about 8 keV above the 992-keV resonance. The existence of this resonance was ignored in all the calculations.

For the targets E-2 through E-6, an analyzer resolution of 0.02% was used, and for targets E-1 and E-7, an

analyzer resolution of 0.05% was used. It has been our experience that a theoretical analyzer resolution of 0.05% does not occur in practice because, when the slit is this wide, the effective distribution of particle energies at the input to the electrostatic analyzer is not uniform.[5] Thus, the true beam-energy resolution for targets E-1 and E-7 is not known *a priori*. However, for a resolution of 0.02% the experimental conditions are quite well known; therefore, the comparison of the experimental data with the calculated yield curves was started with target E-6.

Target E-6

The results of the calculation and the normalized datum points are shown in Fig. 4. Curve I results when the target is assumed to be pure aluminum. Curves II and III result when the target is assumed to be fully oxidized, the difference being in the value assigned to $I(Z)$, 125 eV for curve II and 105 eV for curve III. The value $I(Z)=125$ eV is obtained from the geometric average of the ionization potentials of aluminum (165 eV) and oxygen (108 eV). The value $I(Z)=105$ eV is found when one assumes the ionization potential of aluminum to be 150 eV and the ionization potential of oxygen to be 80 eV. These assumed values are not inconsistent with numbers appearing in the literature.[29] The second set of numbers, 150 eV and 80 eV, were used in order to justify forcing a low value of $I(Z)$ for Al_2O_3. This low value was used to test the sensitivity of the shape of the yield curve to the value of $I(Z)$. The agreement between curve II and the data points of Fig. 4 implies that a consistent, but not necessarily unique, set of conditions is that target E-6 is essentially fully oxidized and the value $I(Z)$ for Al_2O_3 is about 125 eV.
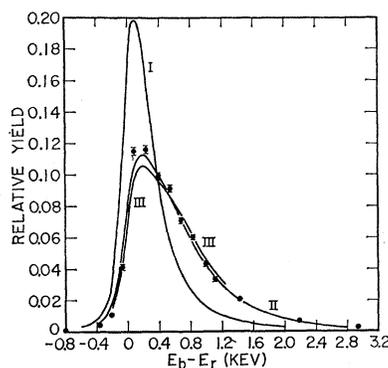

FIG. 4. Theoretical yield curves and data points for target E-6, analyzer resolution 0.02%, 992-keV resonance. Curve I, the target consists of pure aluminum. Curve II, the target consists of pure Al_2O_3, $I(Z)=125$ eV. Curve III, the target consists of pure Al_2O_3, $I(Z)=105$ eV. The enhanced asymmetry of curves II and III is due to the oxidized targets being thicker, resulting in greater fluctuations in energy loss.

[27] H. Bichsel and E. A. Uehling, Phys. Rev. 119, 1670 (1960). These authors give for aluminum $I(Z)=163$ eV. Our value of 165 eV is an arbitrary round-off.

[28] K. J. Broström, T. Huus, and R. Tangen, Phys. Rev. 71, 661 (1947).

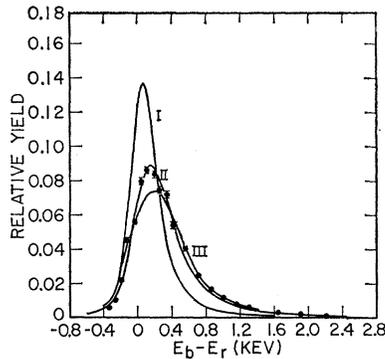[29] S. K. Allison and S. D. Warshaw, Rev. Mod. Phys. 25, 779 (1953).

FIG. 5. Theoretical yield curves and data points for target E-7, analyzer resolution nominally 0.05%, 992-keV resonance. Curve I, the target consists of pure aluminum. Curve II, the target consists of pure Al_2O_3, $I(Z) = 125$ eV, and effective beam-energy spread is 0.03%. Curve III, the same as II except effective beam-energy spread is 0.05%.

Target E-7

Figure 5 illustrates the results pertaining to target E-7. As before, curve I is for a pure aluminum target and an analyzer resolution assumed to be 0.02%. Curves II and III are for a completely oxidized target and for assumed resolutions of 0.03 and 0.05%, respectively. The somewhat better agreement of the data with curve II indicates that the effective analyzer resolution at a setting of 0.05% is substantially better than 0.05%, as expected from previous experience.[5]

Target E-5

The results for target E-5 are shown in Fig. 6. The conditions for the different curves are as follows: curve I, no target oxidation; curve II, the front 20% of the aluminum is fully oxidized, but no other oxidation exists; curve III, the target is 67% oxidized throughout its entire volume. Although the agreement between the
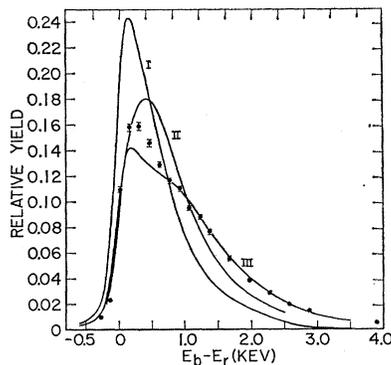

FIG. 6. Theoretical yield curves and data points for target E-5, analyzer resolution 0.02%, 992-keV resonance. Curve I, the target consists of pure aluminum. Curve II, the front 20% of aluminum is completely oxidized, but the rest of the target is pure aluminum. Curve III, the target is 67% oxidized throughout its entire volume. Curve III, representing a thicker target than the others, shows the beginning of the "intermediate-thickness" target characteristics.

experimental points and the calculated curves in the vicinity just above resonance energy is not quite so good as for Figs. 4 and 5, the agreement for curve III at higher energies is as good. Although all three curves represent targets with the same amount of aluminum, the targets they represent are not the same thickness in energy-loss units. That is, if target E-5 had experienced no oxidation, it would have been 1.2 keV thick. Curve III corresponds to a target of thickness 2.0 keV. The three curves illustrate the effects of the different thicknesses. The irregularity of curve III about 1 keV above resonance energy shows the beginning of the characteristics of the "intermediate thickness" uniform composition target.
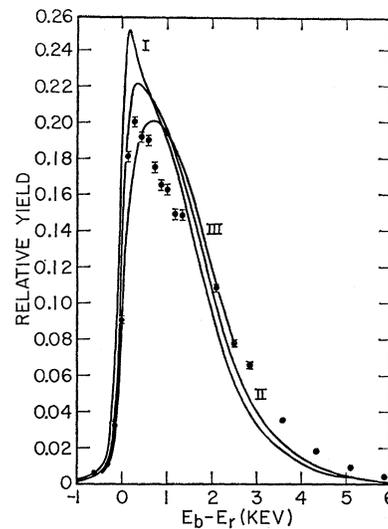

FIG. 7. Theoretical yield curves and data points for target E-4, analyzer resolution 0.02%, 992-keV resonance. The different curves represent different percentages of oxidation confined to the front of the target: I, 0%; II, 5%; III, 10%. Note that the peak for a pure aluminum target (I) is hardly shifted at all from resonance energy. Note also the extra point of inflection of I, characteristic of "intermediate-thickness" targets.

The three curves of Fig. 6 represent three different oxidation conditions for target E-5. It appears likely that some other oxidation condition, perhaps intermediate between II and III, would give significantly better agreement in the vicinity just above resonance energy. No other curve has been computed for such an intermediate oxidation condition because II and III illustrate adequately the basic effect of target composition on yield curve shape.

Targets E-4 and E-3

Figures 7 and 8 show the data and calculated curves for targets E-4 and E-3, respectively. Both of these targets exhibit intermediate thickness characteristics; that is, they show neither the reasonably symmetric shape of really thin targets nor the plateau shape of really thick targets. For the various curves of Figs. 7
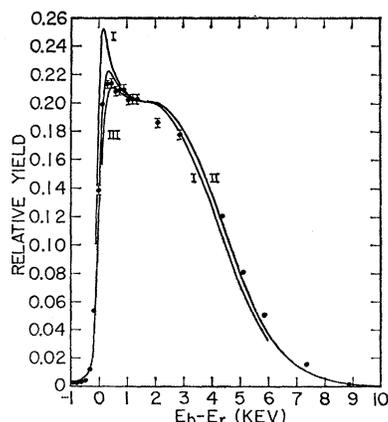
FIG. 8. Theoretical yield curves and data points for target E-3, analyzer resolution 0.02%, 992-keV resonance. The different curves represent different percentages of oxidation confined to the front of the target: I, 0%; II, 2.5%; III, 3.7%. These targets are on the verge of being "thick," but note that the peaks of the curves are still only slightly shifted from resonance energy.

and 8, different percentages of aluminum are assumed to be oxidized. The oxidized aluminum is assumed to be that part near the front face of the target, and in this layer, oxidation is assumed to be complete. The percentages of aluminum assumed to be oxidized are as follows: 7-I, 0%; 7-II, 5%; 7-III, 10%; 8-I, 0%; 8-II, 2.5%; 8-III, 3.7%. Curves 7-II and 7-III do not show the extra point of inflection shown by 7-I because they represent targets whose compositions are not uniform. It appears from the shapes of the various theoretical curves and the experimental curve in Fig. 7 that better agreement would have been obtained if the assumed oxidation had been tapered from 100% near the target face to lower values for the deeper layers. Curve 8-III
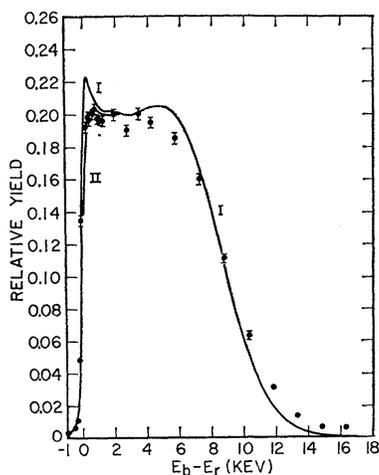

FIG. 9. Theoretical yield curves and data points for target E-2, analyzer resolution 0.02%, 992-keV resonance. The different curves represent different percentages of oxidation confined to the front of the target: I, 1.3%; II, 2.6%. Target E-2 is the thinnest target to show a "thick-target plateau." But as with somewhat thinner targets, the peak is shifted only slightly from resonance energy.

was not computed beyond about 2 keV above E_r because it would not have been significantly different from 8-II. Observe that the peaks of the calculated curves do not shift by an amount equal to half the target thickness, thus agreeing with the experimental data which first demonstrated this anomaly and thereby causing it to be not an anomaly at all!

Targets E-2 and E-1

Figures 9 and 10 show the data and the calculated curves for targets E-2 and E-1, respectively. These targets may be considered to be thick since these curves do exhibit a plateau shape typical of thick targets. The percentages of oxidation assumed (on the same basis as given above for targets E-4 and E-3) are as follows: 9-I, 1.3%; 9-II, 2.6%; 10-I, 0.7%; 10-II, 1.3%.

In some respects the hump may be considered to begin to become apparent with the intermediate thickness targets E-4 and E-3; but those targets are sufficiently thin that the hump appears to be simply the
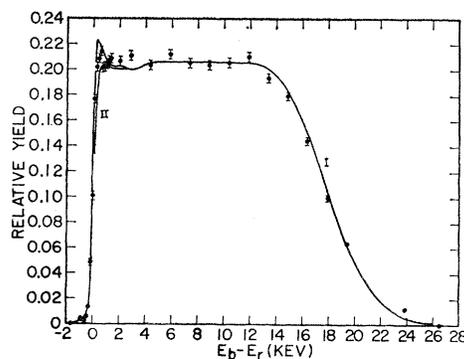

FIG. 10. Theoretical yield curves and data points for target E-1, analyzer resolution nominally 0.05%, 992-keV resonance. The different curves represent different percentages of oxidation confined to the face of the target: I, 0.7%; II, 1.3%.

peak of the curve not displaced much from resonance energy. For targets E-2 and E-1, the calculated curve shows a definite hump. It so happens that the data of target E-2 do not show much of a hump because this target apparently had a significant amount of oxidation on its face. The data for target E-1 do show the hump although not in a pronounced way, and other targets show it better. On the abscissa scale used for Figs. 9 and 10, the different curves tend to merge in all energy regions except the vicinity of the hump. Therefore, only one curve is shown in the higher energy region.

The dip and rise following the hump may or may not be a real effect. The amount of this dip is about 2.5% of the plateau height, and therefore, is rather small. It appears quite probable that the numerical procedures in the integration led to this dip. The size of the hump, in contrast to the size of the dip, is about 25% of the plateau height for a pure target.
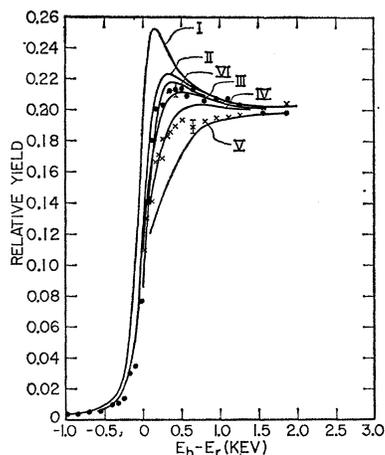
FIG. 11. Theoretical yield curves and data points for "rotated-target" experiment. The target was thick, the analyzer resolution was 0.02%, and the resonance was at 992 keV. The solid circles correspond to the target being 90° to the beam; the crosses, 20°. The different curves I–V represent different thicknesses of surface oxidation: I, 0 eV; II, 260 eV; III, 390 eV; IV, 520 eV; V, 780 eV of Al_2O_3. Curve VI represents a pure aluminum target coated with a layer of C^{12}, 100 eV thick.

5. Comparison of the Integrated Yield Equation with Other Data

Rotated Target

The thick target used for the rotated-target experiment was not one of the E series. The experimental details of this measurement are given in Sec. IV, and the data are shown in Fig. 11 along with several calculated curves. The solid circles represent the data for which the target was perpendicular to the beam, and the crosses represent data for which the plane of the target was at an angle of 20° with respect to the proton beam. The different curves I to V correspond to assumptions of surface oxidation of the aluminum to different thicknesses as follows: I, 0 eV; II, 260 eV; III, 390 eV; IV, 520 eV; V, 780 eV. Curve VI was calculated with the assumption that a layer of C^{12}, 100 eV thick, coated the target, but no oxidation existed. The rotation of the target in the experimental arrangement should have caused whatever layer of contaminant that existed on the target to increase a factor of three in effective thickness. The oxide layer assumed for curve V was a factor of three thicker than that for curve II. A visual inspection indicates that the apparent change in oxide layer thickness for the experimental data was less than this factor of three, but qualitatively the calculations explain the change in shape for the two different experimental conditions. Note the relative effectiveness of C^{12} and Al_2O_3 in depressing the hump.

The abscissa scale of Fig. 11 allows one to see the displacement from resonance energy of the midpoint of the rise for the pure target. The amount of this displacement can be seen to be 100 eV for the pure target, while the displacement is near zero for the coated and

partially oxidized targets, and is in the opposite direction for the thicker contaminant layers. Thus, for a target that is slightly dirty, there may be no displacement!

It is also of interest to note that the slope of the rise in the calculated thick-target yield curve is less when the target surface is contaminated than when only pure aluminum is assumed. This effect explains qualitatively the old vs new target data, in which the old target always showed a greater interquartile width than did the new target.

1317-keV Resonance

Figure 12 shows the experimental data and two calculated curves for the 1317-keV resonance and a thick aluminum target. Curve I represents a pure aluminum target, and curve II corresponds to a target with a 340-eV-thick Al_2O_3 layer on its surface. The experimental resolution was 0.01%, and the intrinsic resonance width Γ was assumed to be 50 eV because the experimental data indicated a narrower width for the 1317-keV resonance than for the 992-keV resonance. The hump is clearly visible in both the experimental data and the calculated curves.

1843-keV Resonance in the $Ni^{58}(p,\gamma)Cu^{59}$ Reaction

An electroplated target of Ni^{58} was prepared and was believed to be about 5 keV thick; but when it was used for measurements of the gamma-ray yield from the 1843-keV resonance, the resulting yield curve shape did not have the appearance typical of a thick target, as can be seen in Fig. 13. The target thus appeared to be inferior even though we had believed it to be one of our best. However, the shape of the yield curve can be fully explained by the integration of the yield equation. Curve I was computed under the assumption of a pure Ni^{58} target, 5.3 keV thick, an intrinsic resonance width
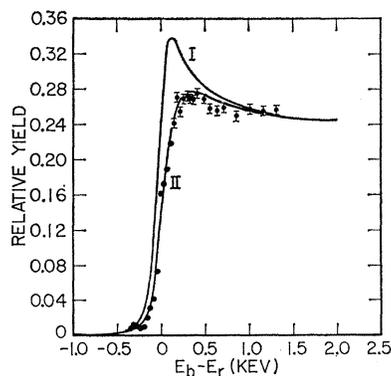

FIG. 12. Theoretical yield curves and data points for a thick aluminum target, analyzer resolution 0.01%, 1317-keV resonance. Curve I represents a pure aluminum target, and curve II represents a target with a 340-eV layer of Al_2O_3 on its surface. Note that the midpoint of the rise of I is about 60 eV below resonance energy, but the midpoint of the rise of II, corresponding more closely to experiment, is almost exactly at resonance energy.
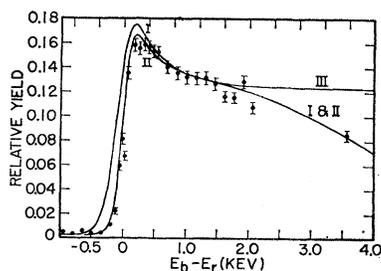
Fig. 13. Theoretical yield curves and data points for a 5-keV Ni^{58} target, analyzer resolution 0.02%, 1843-keV resonance. Curve I represents a pure nickel target. Curve II represents a pure nickel target coated with a 60-eV layer of C^{12}. Curve III is based on a 10-keV target and is shown to indicate the plateau height of a truly thick target. Note how far the peak is from $E_r + t/2$! Note also how enhanced the hump is compared to the aluminum target humps.

of 50 eV, and a beam resolution of 0.02%. Curve II is the same except for an assumed layer of C^{12}, 60 eV thick, on the target surface.

The enhanced appearance of the hump for the Ni^{58} target is at the expense of the appearance of the plateau. That is, the 5.3-keV Ni^{58} target showed less of a plateau than the 4.7-keV Al^{27} target. Thus the 5.3-keV target, which would ordinarily have been expected to show evidences of being thick, does not do so. For purposes of comparison the plateau height for a thick Ni^{58} target is shown by curve III, Fig. 13.

The difference between the relative heights of the experimental humps for the 992-keV and the 1843-keV resonances is due mainly to the following reasons: (1) the lesser contamination of the Ni^{58} target because of its lower chemical activity, (2) the apparent smaller width Γ of the Ni^{58} resonance, and (3) the higher stopping power of nickel. The theoretical hump height for the 992-keV resonance, based on a beam-energy resolution of 0.02% and a Γ value of 100 eV, is 24% of the plateau height; while for the Ni^{58} resonance, a beam energy resolution of 0.02%, and a Γ value of 50 eV, the theoretical hump height is 41%.

VI. APPLICATION TO RESONANCE-ENERGY DETERMINATION

Figure 7 shows one possible source of error in measuring resonance energies with *thin* targets: that if a correction of half the target thickness is applied to the peak of the yield curve for target E-4 (thickness 2.2 keV) in order to obtain the resonance energy, an error of about 700 eV is introduced into the resonance energy determination because the actual experimental peak is displaced only about 400 eV from resonance energy.

Figure 11 shows a possible source of error in measuring resonance energies with *thick* targets: that the midpoint of the rise of a pure aluminum thick-target curve for the 992-keV resonance is about 100 eV below the true resonance energy. The amount of this displacement of the midpoint of the rise from E_r is dependent upon

Γ, E_r, beam-energy inhomogeneity, target thickness, target stopping power, and target cleanliness and purity. In order to illustrate the way in which this displacement varies with Γ, we have computed the amount of the displacement as a function of Γ with the following conditions: target E-2 (about 9 keV thick and assumed to be pure aluminum), 992-keV resonance, and a beam-energy resolution of 0.02%. Figure 14 shows the resulting curve. Observe that there is a particular value of Γ (about 1 keV) leading to a maximum displacement. The drop in the curve at values greater than $\Gamma = 1.0$ keV is somewhat faster than if a thicker target had been used in the calculation; i.e., a 9-keV-thick target is too thin for a good determination of the thick-target yield-curve shape for resonance widths greater than about 1 keV.

The considerations presented in the preceding two paragraphs indicate that the most accurate method for determining the resonance energy of a very narrow resonance is to use neither of the above procedures but to calculate the yield curve as described herein and to compare this calculated curve with the experimental curve.

For each target of the E series, the calculated curve showing the best agreement with the data (Figs. 4 and 10) was used to determine E_r. Visual adjustment of the abscissas of the experimental and calculated curves provided the means of choosing a value of E_r for that particular target. In this way, the maximum degree of judgment was exercised on the conditions of target purity and other factors influencing the experimental data. The arithmetic average of the seven values is 991.91 ± 0.30 keV. The uncertainty given here is the absolute uncertainty in the energy determination and is found by calculating the square root of the sum of the squares of the individual uncertainties of the various parameters related to the separate components of the electrostatic analyzer.[5]

The data of the target E-1 from the present series of experiments are the same data that were included in a previous communication[6] reporting the $T^3(p,n)He^3$ threshold-energy measurement. In that paper, the value of the bombarding energy at the midpoint of the rise of the thick-target step was reported to be 992.0 keV. This
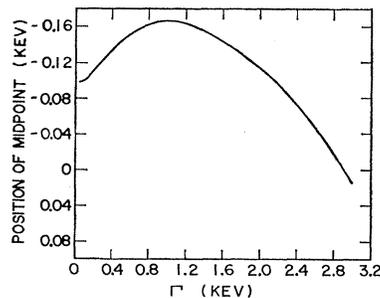

Fig. 14. Displacement (E_b at midpoint minus E_r) of the midpoint of the rise of a thick-target yield curve as a function of Γ. The assumed parameters are a 9-keV pure aluminum target, $E_r = 992$ keV, and an analyzer resolution of 0.02%. Note that the displacement is not a monotonic function of Γ.

Table I. List of best values of absolute resonance energies for a number of narrow (p,γ) resonances. These values were obtained by the fitting of theoretical yield curves for each resonance to the experimental data, and therefore, include a judicious choice for quantities usually ignored, such as the degree of oxidation of the target and the presence of an inert contaminating layer over the target as well as fluctuations in energy loss. The uncertainties are in the absolute values.

Reaction	Resonance energy (keV)
$Al^{27}(p,\gamma)Si^{28}$	991.91 ± 0.30
$Al^{27}(p,\gamma)Si^{28}$	1317.19 ± 0.40
$C^{13}(p,\gamma)N^{14}$	1747.06 ± 0.53
$Ni^{58}(p,\gamma)Cu^{59}$	1423.64 ± 0.43
$Ni^{58}(p,\gamma)Cu^{59}$	1843.45 ± 0.56

value was rounded up from 991.95 keV. It should be emphasized that the data reported herein, and illustrated in Fig. 10, are the same data as previously reported and that the bombarding energy at the midpoint of the rise for target E-1 is still reported as 991.95 keV. It so happens that the effect of impurity for target E-1 exactly canceled within the precision of the measurements the effect due to fluctuations in energy loss; and therefore, the value of E_r for target E-1 is the same as the energy at the midpoint of the rise, 991.95 keV. So there is no change in our energy calibration subsequent to the $T^3(p,n)He^3$ threshold-energy measurement. The calculated curves were not available at the time of submission of the manuscript of the $T^3(p,n)He^3$ experiment.

We feel justified in assigning equal weight to each of the seven measurements because we have confidence in the method used to compare the data with the calculations. We, therefore, take the value of 991.91 ± 0.30 keV to be our best value of the intrinsic resonance energy E_r.

Best values have been obtained in the same manner for the other resonances discussed herein. These other values are based on thick-target data only. See Table I for a listing of these best values.

VII. APPLICATION TO RESONANCE-WIDTH DETERMINATION

For a given set of conditions, the slope of the rise of the yield curve calculated with Eq. (1) will be greater than when calculated with an equation in which the energy loss of the protons is assumed to be equal to kx, where k is a constant. Thus if the latter assumption is made for the computation of yield curves as a function of Γ, comparison of the experimental data with the slope alone will lead to an anomalously low value for Γ if extremely pure surface conditions exist on the target. For values of Γ greater than several hundred eV there is no serious problem of determining Γ with reasonable precision, e.g., 20%. However, for values of Γ equal to or less than 100 eV the effects of surface contamination on the slope of the rise can introduce uncertainties of 50% or more in the determination of Γ. Thus because of the contamination problem, no effort has been made
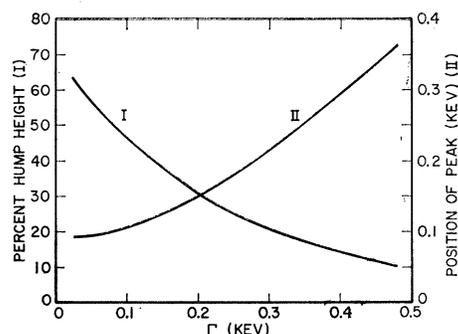

Fig. 15. Curve I (left ordinate) is the theoretical hump height (as a percentage of the plateau height) as a function of Γ. Curve II (right ordinate) is the displacement of the peak of the hump from E_r as a function of Γ. The assumed parameters are a thick pure nickel target, $E_r=1843$ keV, and an analyzer resolution of 0.01%.

in the present work to assign precise values of Γ to the various resonances.

An intriguing possibility is that the experimental height of the hump could be used as a measure of the width of a resonance for targets whose purities were known; that is, the narrower the resonance, the greater the height of the hump. In order to illustrate this idea quantitatively, we have computed the height of the hump for several assumed values of Γ from 25 eV to 500 eV for the following conditions: pure Ni^{58} target, $E_r=1843$ keV, and a beam-energy resolution of 0.01%. These values result in the curve of Fig. 15. The left ordinate (curve I) is the percentage rise of the hump above the plateau of the thick-target yield curve. The right ordinate (curve II) is the displacement of the peak of the hump from resonance energy. Curves of similar shape result if Γ is assumed constant and the height of the hump is determined as a function of beam-energy resolution. Conversely, if the resonance width is known, or if there exists an uncontaminated target, the height of the hump can be used as a measure of the depth of oxidation or degree of contamination.

The theoretical hump height has been computed for resonances in other materials. For the $C^{13}(p,\gamma)$ resonance at 1747 keV, an assumed Γ of 80 eV, and a beam-energy resolution of 0.01%, the theoretical hump height is 17%. The observed hump height was 7%. The stopping power, dE/dx, for protons of 1747 keV on $C^{13}-C^{12}$ is about 330 MeV/cm, and for protons of 1843 keV on Ni^{58} the stopping power is about 810 MeV/cm. For the Ni^{58} case the theoretical hump height is 56% and the observed hump height is 28%. Thus, we see a correlation between stopping power and theoretical hump height, the higher stopping power leading to a higher hump.

VIII. DISCUSSION

1. Related Work

The existence of one of the anomalies reported herein, the presence of a hump on the thick-target yield curve, was found by del Callar.[9] In the meantime, the existence of the hump was predicted by Lewis[15] and was observed

experimentally by the Wisconsin group.[14,18] However, they failed to demonstrate that the presence of the hump was not due to some experimental flaw such as a thin-target yield curve superimposed on a thick-target yield curve (see Sec. IV).

The explanation of the hump given by Lewis[15] appears at first to be quite different from that given herein. However, the two methods are fundamentally very similar. To calculate a thick-target yield curve, the Wisconsin group assumes that the single-collision cross section is applicable between values of some E_{max} and some E_{min}. They assign a maximum energy transfer E_{max} (based on the assumption of free electrons) and a minimum energy transfer E_{min} (based on the assumption that electrons bound in aluminum cannot be excited by an energy transfer less than 12.3 eV). By a Monte Carlo calculation, Walters et al.[18] determined the beam-energy distribution effective throughout the volume of a thick target. This result they present in the form of a histogram showing the fraction of incident protons spending any time in each of many energy intervals (Fig. 6, reference 18).

To compare Lewis' approach with our application of Symon's theory, we computed, using the distribution curves of Symon, the proton energy distribution throughout the volume of a thick aluminum target on which is incident a perfectly homogeneous beam. The spectral distribution thus obtained was essentially identical to that of Fig. 6, reference 18. Therefore, it appears that Lewis' approach is equivalent to that of Symon. It is reasonable to conclude that the result is not critically related to the value chosen for E_{min}. Landau's distribution, used in the region of its applicability, plus a constant energy-loss process beyond this region would result in a very similar spectral distribution throughout the volume of a thick target. Thus all of the anomalies can be explained, at least qualitatively, by the application of Landau's distribution only. It might be noted that above some small value of energy loss, the Landau distribution and the single-collision cross section are very nearly the same. Thus, there is greater similarity between the approach of Lewis and that used herein than at first appears to be the case. It appears likely that the computational method of Lewis would also satisfy the experimental observations herein concerning the failure of the peaks of thin-target yield curves to shift as much as half the target thickness.

The Wisconsin calculated yield curves showed a displacement of the midpoint of the rise of the thick-target yield curve to energies below resonance energy in general agreement with the present results. However, the conclusions drawn in the present paper concerning the amount of the displacement observed in practice are significantly different.

One other point covered in common by the Wisconsin results and those given herein concerns the interquartile interval for thick-target yield curves. Walters et al.[18] found that targets having the same interquartile inter-val were sufficiently different that one showed the thick-target hump and the other did not. This observation is in disagreement with the results reported herein for aged targets and rotated targets. We found that the interquartile interval is as sensitive to impurities and contaminants as the hump. So if one target shows a hump and another does not, then the interquartile intervals will be significantly different.

2. Recapitulation

A number of anomalies in (p,γ) yield curves have been observed with H_1^+ beams on targets of different thicknesses. The most striking of these anomalies is the fact that the peaks of the yield curves of moderately thin targets do not shift from true resonance energy by an energy that is even comparable with half the target thickness. Most of the other anomalies observed are simply different manifestations of this anomaly. These and all other anomalies observed with H_1^+ beams have been explained by the application of the theory of fluctuations in energy loss, including target contamination effects. The most important feature of this theory is that the most probable energy loss for thin layers is usually much less than the average energy loss, resulting in an asymmetric energy-loss distribution with its peak near zero. Using this theory we have succeeded in calculating yield curves which are in excellent agreement with the experimental data for all target thicknesses.

This entire series of experiments was initiated by observations made in the course of a program of preparing a new absolute precision energy scale for nuclear-reaction accelerators. At one time it appeared that the instrumental precision significantly exceeded the precision of interpretation of the results, primarily because of the lack of a detailed understanding of the interactions in the atomic, rather than the nuclear, domain. The success of the theoretical interpretations herein implies that these interactions are now sufficiently well understood that one can take full advantage of all available instrumental precision.